

Pianta, Nicolò ; Scarpioni, Federico ; Chukwu, Richard ; La Mantia, Fabio ; Ruffo, Riccardo



Evaluation of kinetic parameters of non-faradic processes in carbon-based electrodes using multisine dynamic electrochemical impedance spectroscopy

Journal Article as: peer-reviewed accepted version (Postprint)

DOI of this document* (secondary publication): <https://doi.org/10.26092/elib/3664>

Publication date of this document: 14/02/2025

* for better findability or for reliable citation

Recommended Citation (primary publication/Version of Record) incl. DOI:

Nicolò Pianta, Federico Scarpioni, Richard Chukwu, Fabio La Mantia, Riccardo Ruffo, Evaluation of kinetic parameters of non-faradic processes in carbon-based electrodes using multisine dynamic electrochemical impedance spectroscopy, *Electrochimica Acta*, Volume 437, 2023, 141462, ISSN 0013-4686, <https://doi.org/10.1016/j.electacta.2022.141462>.



Please note that the version of this document may differ from the final published version (Version of Record/primary publication) in terms of copy-editing, pagination, publication date and DOI. Please cite the version that you actually used. Before citing, you are also advised to check the publisher's website for any subsequent corrections or retractions (see also <https://retractionwatch.com/>).

This document is made available under a Creative Commons licence.

The license information is available online: <https://creativecommons.org/licenses/by-nc-nd/4.0/>

Take down policy

If you believe that this document or any material on this site infringes copyright, please contact publizieren@suub.uni-bremen.de with full details and we will remove access to the material.

Evaluation of kinetic parameters of non-faradic processes in carbon-based electrodes using multisine dynamic electrochemical impedance spectroscopy

Nicolò Pianta^{a,*}, Federico Scarpioni^b, Richard Chukwu^c, Fabio La Mantia^{b,c}, Riccardo Ruffo^a

^a Department of Materials Science, University of Milano Bicocca, via R. Cozzi 55, Milan I-20125, Italy

^b Fraunhofer Institute for Manufacturing Technology and Advanced Materials IFAM, Wiener Strasse 12, Bremen 28359, Germany

^c Faculty of Production Engineering, Energy Storage and Energy Conversion Systems, Bremen University, Wiener Strasse 12, Bremen 28359, Germany

ARTICLE INFO

Keywords:

Dynamic impedance spectroscopy
Dynamic multi-frequency analysis
Electrochemical double-layer capacitors
Three-electrode cell
Equivalent circuit modelling

ABSTRACT

Dynamic Electrochemical Impedance Spectroscopy is a valuable tool to investigate kinetic parameters of non-Faradic processes in symmetric Electrochemical Double Layer Capacitors. Compared to classic Electrochemical Impedance Spectroscopy, the dynamic technique measures the impedance under non-equilibrium condition removing the stationarity requirement and, at the same time, giving the frequency-dependent information of a dynamic process in presence of overpotential. Despite not being a new technique, there is an inherent complexity in the signal sampling and data manipulation to obtain the impedance spectra down to low frequencies (the interesting band for energy storage devices impedance). Few methods to compute the impedance from sampled signals are reported in the literature and under development. For this work the Dynamic Multi-Frequency Analysis algorithm was used to compute the impedance and reconstruct the cyclic voltammetry profile as well. The time-dependency of the kinetic parameters, namely capacitances of double layer and adsorption phenomenon, were extracted from equivalent circuit model regression and the adsorption time constants with a graphical analysis of the impedance spectra dataset during a full charge/discharge cycle. The values of the adsorption capacitance from the model regression are, on average, compatible with the values computed with a common formula showing the reliability of the model regression. The use of a three-electrode compact cell allowed the characterization of both active electrodes independently during operation showing a strong potential dependence on the active material properties. Furthermore, the impedance showed the presence of a side reaction (likely oxygen evolution) connected to the increase of adsorption and double layer capacitances localized on the positive electrode in a clearer way than what was possible to observe from the voltametric profile.

1. Introduction

Electrochemical Double-Layer Capacitors (EDLCs) are a class of devices that store energy at the interface between electrode and electrolyte in the form of electrostatic energy. This allows them to position themselves midway between common capacitors and alkali-ion batteries in terms of energy density, power density and cycle life [1,2]. The fast-charging process makes them suitable for applications where high cycle life and power are of the utmost importance without neglecting the energy density [3]. EDLCs can, in fact, be charged/discharged about 10 times faster than lithium-ion batteries [4], at the cost of one order of magnitude in energy density, thus drastically increasing the delivered power.

In EDLCs and, in general, in any electrochemical system, several processes happen at the electrode/electrolyte interface; some of them are intended for the function of the device while others may be unwanted and can deteriorate its performance over time. Identifying and quantifying their kinetics parameters for device optimization or fundamental studies require looking at the problem from different angles. A set of experimental techniques are available in electrochemistry to characterize different aspects of the system at the equilibrium or out of it. These techniques include constant and linear sweep chronoamperometry and chrono-potentiometry, and frequency dependent techniques, among which Electrochemical Impedance Spectroscopy (EIS) [5] is one of the most common. EIS is a non-invasive technique that allows the detection and quantification of the kinetic processes in

* Corresponding author.

E-mail address: n.pianta@campus.unimib.it (N. Pianta).

electrochemical systems (e.g. charge transfer, double-layer formation, diffusion in liquid and solid phases). The impedance response of an energy storage device can be used as operation control, diagnostic tool, modelling and materials characterization [6–9]. From the impedance characteristic, different properties of the EDLCs can be extrapolated; in literature two important effects are reported: (i) the relationship between interface capacitance and porosity or electrolyte resistance [10]; (ii) the effect of the conductive filler in the electrode formulation to the electrochemical performance [11]. Moreover, EIS measurements were used to study electrodes aging [12] and to define a charge/discharge prediction model [13].

The classic EIS experiment uses stepped frequency sine waves as perturbation to obtain the impedance spectra over multiple decades. This approach is well known and established with great accuracy and low noise. The system, however, must not change during the impedance acquisition so to satisfy the stationarity requirement [14]. Electrochemical systems are, in fact, prone to changes in operative conditions due to environmental effect (e.g. temperature drift) or relaxation. At the cost of a greater noise, the time required for a single impedance experiment can be reduced using a multi-sine broadband perturbation made of the algebraic sum of many sine waves with different frequencies. Starting from the concept of multi-component perturbations, the idea of measuring the time-varying impedance of a system during a controlled drifting of the system by superimposing the multi-sine perturbation on another signal of choice, like sweeping potential [15], constant current [16] or potential [17] or even in presence of tensile stress [18] was developed. The combined technique is generally referred to as Dynamic Electrochemical Impedance Spectroscopy (DEIS).

Various methods to compute the impedance spectra starting from multi-component potential and current signals were proposed among the years, which can be divided in two categories: (i) numerical and (ii) analytical methods. Both methods make the use of Fourier analysis to separate the perturbation components (i.e. main drift and sine waves with different frequencies that compose the multi-sine wave). Numerical methods rely on windowing or filtering the signals in time or frequency domain, respectively (the techniques are referred to as STFT-EIS and DMFA [19]) before computing the discrete valued time-varying impedance. Analytical methods, on the other hand, aim to obtain the analytical function that describe the frequency-dependent time-varying impedance from the regression of a model function to the transformed signals (i.e. shape of the frequency domain peaks relative to each perturbation) [20]. A review of some of the available methods was made by Szekeres et al. [21].

Aim of this paper is to use Dynamic Electrochemical Impedance Spectroscopy and equivalent circuit regression of the obtained spectra to extract the temporal variation of the kinetic parameters for the non-Faradic process occurring in carbon-based electrodes for electrochemical double-layer application under linear sweep chronopotentiometry drifting. To compute the time-varying impedance Dynamic Multi-Frequency Analysis (DMFA) was chosen as an easy-implementable approach in any programming language while still effective in the sub-Hz frequency region of interest. A peculiarity of the presented method is the use of a three-electrode set-up in compact cell format to measure the independent impedance response of positive and negative electrodes.

2. Experimental

2.1. Design and preparation of the electrochemical cells

In the present work, a T-shaped three-way Swagelok type casing was used to assemble a three-electrode compact cell. Self-standing activated carbon electrodes were prepared according to our previous work [22] (1.54 cm² disks, 23.5 mg of active material) put in contact with a glass microfiber separator soaked with an aqueous solution of 10m KF (Sigma Aldrich, 99%+) that allows the use of a lead strip (Goodfellow, 99.99%)

coated with lead fluoride as reference electrode [23]. Despite being more toxic than a conventional AgCl/Ag (Ag: Goodfellow, 99.99%) electrode, the PbF₂/Pb has the important advantage of having a precise and stable potential when placed in contact with a solution that contains fluoride ions, which does not oxidize to F₂ in the potential window of interest. Furthermore, the use of a reference electrode directly in contact with the solution (i.e. no glass bodies and porous junctions) makes the assembly of the aforementioned cell much simpler. Considering the pH of the solution (10.7), a PbF₂/Pb electrode in contact with it present a potential of 191 mV vs RHE. The cells, schematized in Fig. 1, consisted in a PEEK body, with stainless steel pistons pressing the components together. The reference electrodes were inserted in the third and perpendicular way, two positions were tested; the discussion is given in the next session. The cell analyzed with DEIS was pre-treated with cyclic voltammetry (8 mV s⁻¹) until stabilization (i.e. cycles almost the same to each other).

2.2. Instrumental aspects and parameters choice

The potential and current signals were measured by an experimental apparatus made with the combination of the following commercial instruments: (i) a potentiostat for the potential or current control (BioLogic SP-300, 2 channels); (ii) an arbitrary waveform generator for the multi-sine perturbation (Keysight True-Form, 16MSa memory); (iii) a digital oscilloscope for data sampling (PicoScope 4000A, 8 channels, 12bit resolution). The potentiostat was controlled from the proprietary BioLogic EC-Lab Express software that allows summing an external signal input to the internal generator. The connections and the role of each instrument are reported in Fig. 2. In order to measure the potential (and, from it, the impedance) of the two active electrodes vs a reference while sweeping the cell potential, two channels were used simultaneously: the first one between the two symmetric active carbon electrodes to impose an offset potential and the other between the positive electrode and the reference to measure its state-of-charge dependent open-circuit potential; the negative electrode's potential was then calculated as the difference of the cell potential and the positive electrode's one. The waveform generator was used to generate both the multi-sine for EIS probing and the quasi-triangular perturbation for the CV (using the “combine channel” feature of the instrument), while the potentiostat had the role of converting the generator's signal into a voltage one to be used on the cell. Generating the whole input signal with the waveform generator is preferable compared to using the potentiostat to impose the sweeping potential (i.e. CV potential sweep) because of the presence of a filter at the end of the dedicated waveform generator that guarantee a high-resolution analog wave synthesis. The multi-sine perturbation on the arbitrary waveform generator was designed based on previous work [24] with a base frequency of 100 mHz

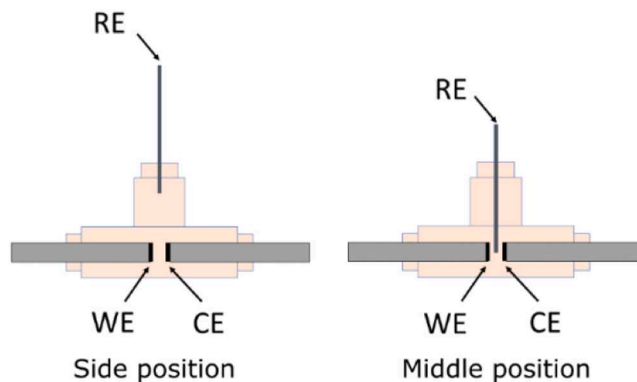


Fig. 1. Schematic section view of the three-way Swagelok-type cell used in this work. The two drawings show the tested positions of the reference electrode in respect to the other two active electrodes.

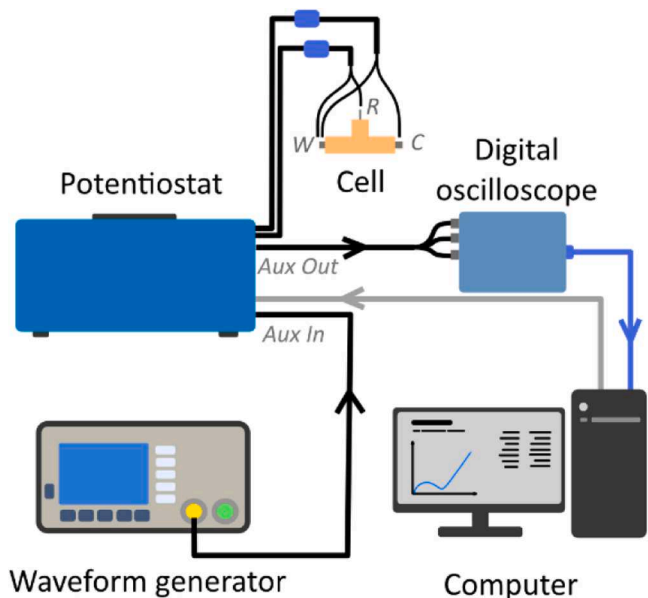


Fig. 2. Schematic draw of the experimental apparatus used to measure the potentials and current to compute the dynamic impedance of the system.

(frequency range from 100 mHz to 100 kHz).

2.3. Time-varying impedance computation

The computation of the time-varying impedance was carried out with the Dynamic Multi-Frequency Analysis (DMFA). The DMFA routine performs a band-pass filtering in the frequency domain of an interval of points around each peak corresponding to a perturbation component (i. e. single frequency component of the multisine or cyclic voltammetry component) [24]. The inverse of the filter bandwidth is the time span during which the impedance is measured as an average, exactly as in a short-time Fourier Transform EIS (STFT-EIS) [19]. To guarantee the independency of two consecutive impedances, the time step between two impedance computation should be an integer multiple of the reciprocal of the filter bandwidth [25]; in the elaboration for this work, 1 was used as the integer resulting in a time of averaging of the impedance equal to 10 s. The DMFA has also the interesting feature of being able to reconstruct the time profile of the cell potential and current centring the filter at zero in the frequency space; having more points here, the time resolution of the DMFA was lowered to 1 s. The parameter “n” of the filter [19] was chosen to be 8 for best results [25]. The procedure is schematically shown in Fig. 3 and more details on the method can be found in previous literature [19,24]. A Python implementation of the DMFA has been developed by the authors and made publicly available [doi: 10.6084/m9.figshare.21081994].

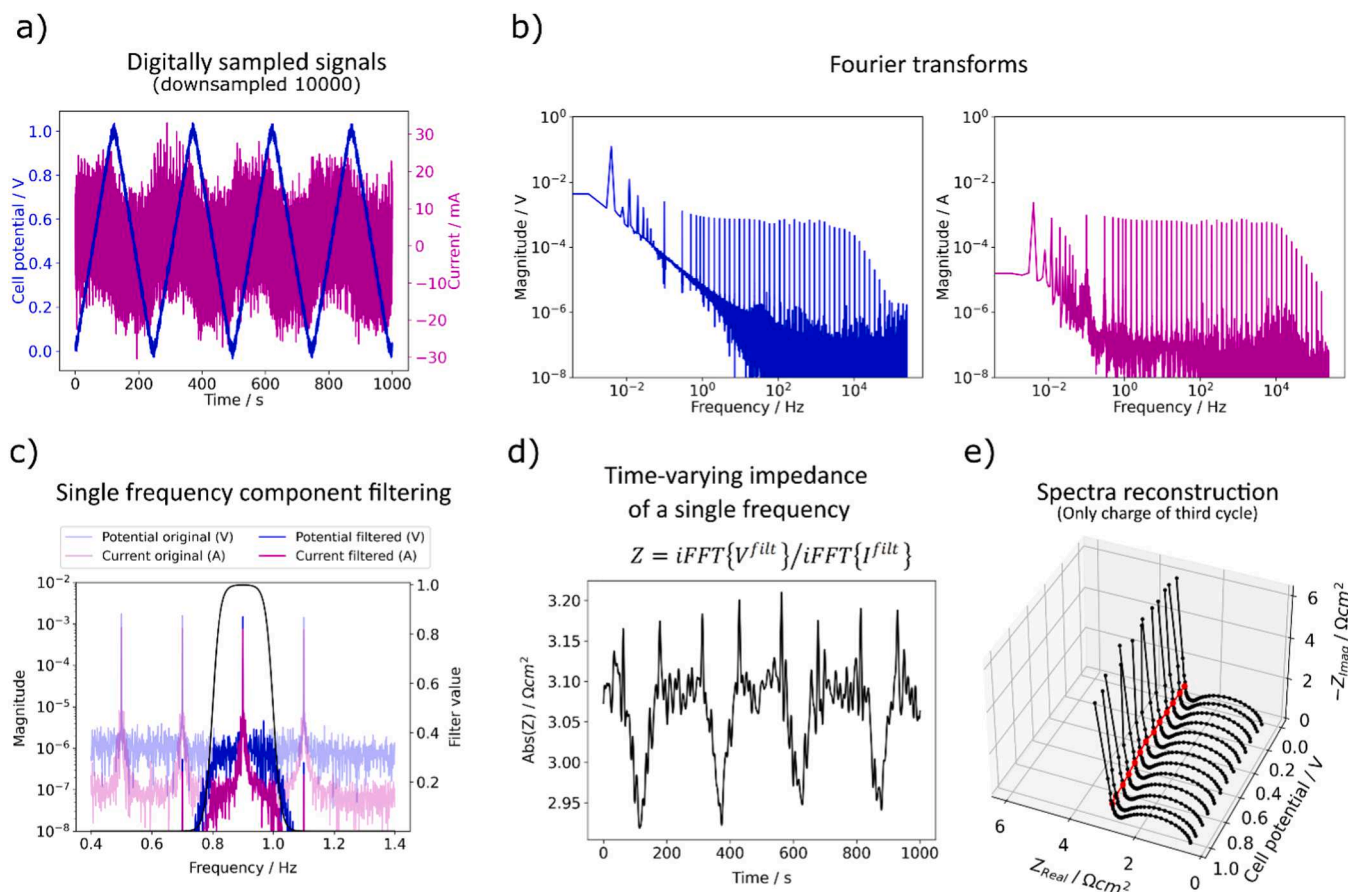


Fig. 3. Graphical representation of the Dynamic Multi-Frequency Analysis: (a) digitally sampled cell current and potential of the cell; (b) Fourier transform of the two signals; (c) filtering of a frequency peak (i.e. the sine component with a frequency of 0.9 Hz in the multi-sine wave), the semi-transparent lines are the original signal while the solid color is the result of the filtering; the filter profile is also reported in black; (d) time-trend of the module of the impedance referred to a single frequency (0.9 Hz), the formula to compute the impedance is reported below the plot; (e) full time-varying impedance for the third charge of the device plotted against the electrode potential (highlighted in red the impedance value at 0.9 Hz).

3. Results and discussion

3.1. The position of the reference electrode

To evaluate the effect of the reference electrode's position on the impedance results and on possible artefacts, two Swagelok cells were assembled and tested with a classic EIS experiment on a logarithmically spaced range between 100 kHz and 100 mHz: one with the reference as far as possible from the active carbon electrodes (flooding the upper chamber of the cell) and one with it in the middle of the other two; Fig. 2 shows schematically the positioning. The position of the reference is widely discussed in the literature and it is strongly dependent on the type of cell in use: flooded or compact [26–29]. In general, the reference electrode should be placed as close as possible to the working electrode to probe the same equipotential line but sufficiently far from the current lines so to avoid surface alteration and the consequent potential drift. In compact cells the available positions for the electrode are even more limited and the electrode/electrolyte contact not trivial to guarantee. In Fig. 4 it can be seen that positioning the reference electrode far from the other two brings a distortion in the mid-to-low frequency region (from about 100 mHz to 1 Hz). Such effect is, on the other hand, strongly limited when positioning the electrode in between the active carbon electrodes, making it the preferable setup, with the second advantage of reducing the amount of electrolyte needed to contact every electrode.

3.2. Dynamic multi-frequency analysis

In the reported experiment, 4 cycles of CV with a superimposed multi-sine perturbation were acquired with a sampling rate of 500 kHz so to reconstruct the higher frequencies. The measurement was performed over a time of 1000 s to have a frequency resolution of 1 mHz and being able to see the very low frequency components. The raw data are made publicly available [doi: 10.6084/m9.figshare.21082168]. The estimation of the multi-frequency response of the system carried out with the DMFA is reported in Fig. 5 for the third cycle of the set. Both CV profiles and time-varying impedance are reported for the single electrodes and the full cell. In the impedance spectra, the 100 mHz frequency point was removed because it was biased by the interacting of the drift frequency skirt. In fact, as shown in Fig. 6, the left side of the relative peak is disturbed and the filtering procedure of the DMFA fails to provide an accurate estimation. In case of EDLCs and energy storage devices in general, the low frequency band down to 10 mHz, or even 1

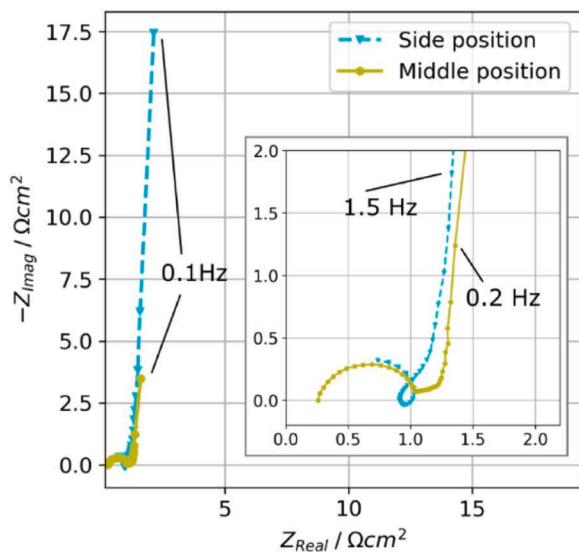


Fig. 4. Classic impedance spectra measured on two cells with different positions of the reference electrode (see Fig. 1 as reference for the positions tested).

mHz, contains useful information on the kinetics but this time scale generally interferes with the drift. The user must take care of a proper multi-sine design depending on the desired experiment and compromise between the lowest frequency and the drift time scale. Here, the quasi-CV scan rate was chosen to be 8 mV s^{-1} , which means a period of 250 s, already pretty short for a device of this kind and hence was selected by the authors as the lower limit to keep the CV analysis meaningful and comparable with previous work in the literature. In Fig. 7 the spectra at zero cell potential for the 3 time-varying datasets as comparison of the magnitude are reported. The difference between the two carbon electrodes' impedance is attributable to the pre-treatment cycles that were performed to stabilize the system, which modified the electrode/electrolyte interface most likely because of a difference in the species adsorbed on the two electrodes.

3.3. Extracting kinetic through regression of equivalent circuits

The time-varying impedances extracted with DMFA can be used to evaluate several kinetic parameters of the electrochemical system (e.g. charge transfer resistances, double-layer capacitances, diffusion coefficients, etc.). One of the approaches to get quantitative information on the electrode kinetics is the mathematical regression of an equivalent circuit (EC) to the experimental data. A typical EC suitable to describe the kinetics of nanoporous activated carbon electrodes is presented in Fig. 8a [30]. The process of charge accumulation or depletion at the double layer is in parallel with the adsorption in the pores while the semi-infinite Warburg element describes the diffusion of the ion from the bulk to the interface. The double layer capacitance of a solid-state electrolyte is described by a constant phase element (CPE) [31]. This circuit fits correctly the impedance of the positive electrode (see Fig. 8c) but not that of the negative one. In fact, it can be seen from Figs. 7 and 8d that a 45° feature is present after the semicircle. Here the semi-infinite diffusion seems not to be the involved process (insufficient model) but rather a finite-space diffusion. An alternative circuit including a finite space Warburg (FSW) element was introduced in place of the adsorption capacitance and the semi-infinite Warburg in series. The FSW element represents the diffusion from a small distance and it was reported to describe the diffusion of solvated ions in close pore systems [32] or the surface diffusion of adsorbed ions [33]. On the negative electrode, hence, the finite-space diffusion process happens at a faster rate than the ion diffusion in the liquid (described with the semi-infinite Warburg in the circuit used for the positive electrode). Using the same circuit as a regression model for the impedance spectra of the positive electrode gives a worse result in terms of regression quality rating given by the Akaike information criterion (AIC) [34].

Fig. 9 shows the double layer CPE effective capacitance for both electrodes computed using regression parameters in the equation proposed by Hirschorn et al. [35]:

$$\text{Eq. (1)}$$

$$C_{\text{eff}} = Q_{0,ad}^{\frac{1}{n}} R_{ad}^{\frac{1-n}{n}} \quad (1)$$

while Fig. 10 shows the adsorption and diffusion capacitances for positive and negative electrodes, respectively obtained directly from the model regression. It is clear that the processes occurring at the interface are strongly dependent on the history of the electrode. The effective capacitance representing the charge accumulation on the double layer is constant until the current in the cell is increased by the electrolyte degradation approaching 1.2V vs RHE for the positive electrode. Instead, the adsorption capacitances increase monotonously with the state of charge with an inverse proportion to the potential scan, except for the positive electrode where the side reaction is taking place and a local accumulation of ion is expected (see Fig. 10). It is interesting to notice that with a DEIS experiment it is possible to highlight the presence of the side reactions on a specific electrode thanks to the time-varying nature of the impedance and the ability to extract the

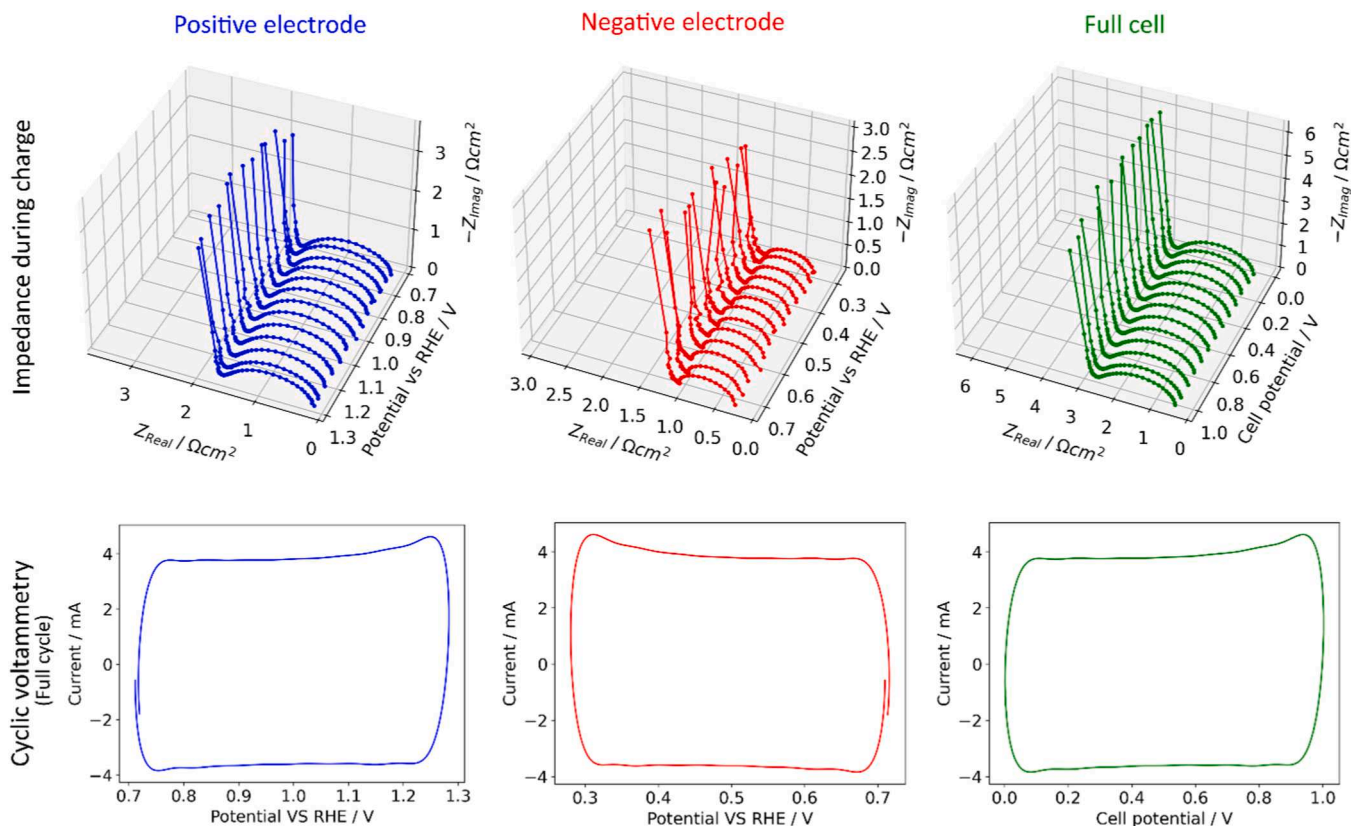


Fig. 5. Time-varying impedance and cyclic voltammetry profiles extracted with DMFA. Impedance spectra are reported only for the charging process due to the high symmetry of the system response.

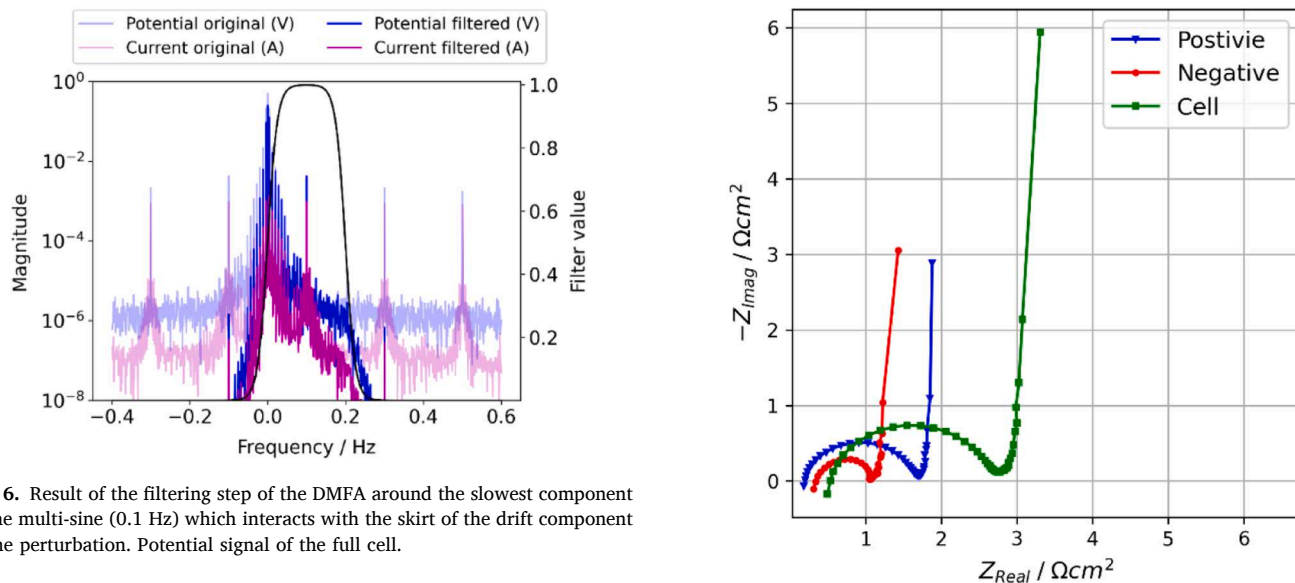


Fig. 6. Result of the filtering step of the DMFA around the slowest component of the multi-sine (0.1 Hz) which interacts with the skirt of the drift component of the perturbation. Potential signal of the full cell.

evolution of the kinetic parameters. On the contrary, from just the CV profile an increase in current is present approaching the extremes of the potential span for both electrode, which are in series, leaving the uncertainty of where the reaction is taking place. This can be useful for more complex systems, where the identity of the side process is not as obvious as it is in the reported example.

The average adsorption capacitances are 44.5 F g^{-1} for the positive and 47.6 F g^{-1} for the negative electrode, which are in accordance with the values obtained from the average capacitances calculated from the extracted CV profile:

$$\text{Eq. (2)}$$

$$C_{\text{average}} = \frac{I}{\frac{dV}{dt}} \quad (2)$$

resulting to be 42 and 54 F g^{-1} for positive and negative electrode, respectively.

For the EC model regression, the datasets were cleaned up removing

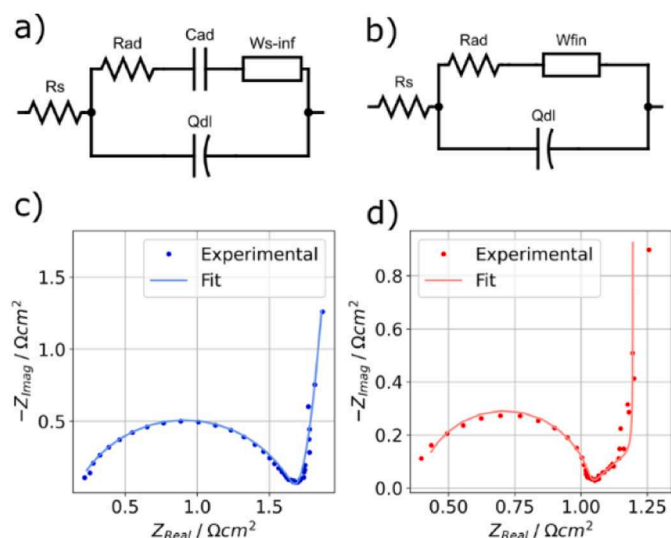


Fig. 8. (a) and (b) Equivalent circuits and (b) and (c) visual regression results for positive (blue) and negative (red) electrode, respectively.

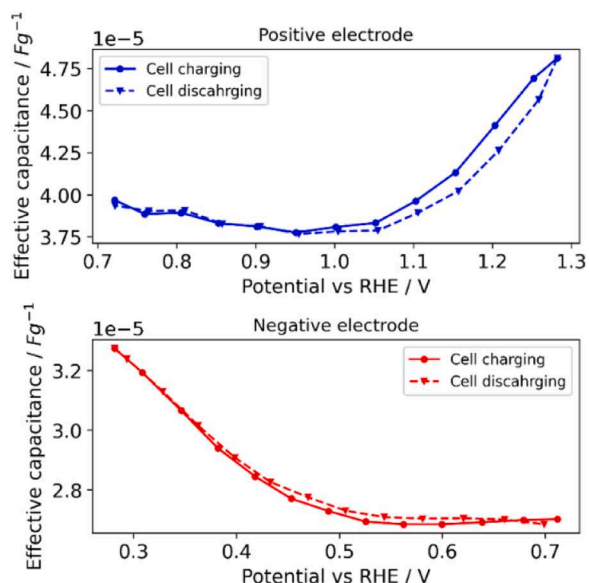


Fig. 9. Double layer effective capacitance computed with Eq. (1) from the parameters extracted with equivalent circuit model regression for both electrodes. Note that positive electrode potential spans from low to high during the device's charge while the one for the negative spans from high to low.

3 frequency points at high frequency that show an inductive behavior and the lowest frequency (100 mHz) which is biased by a big error due to the insufficient spectral separation from the drift components (this can be seen from the Fourier transform of the raw signals in Fig. 3).

3.4. Graphical analysis of imaginary impedance

The extracted impedance data were also used to make some considerations on the time constants, in this case related to the adsorption process. This was done by observation of the imaginary part of the impedances, which have the advantages to show time constants as peaks [36,37], reported versus time (i.e. inverse of the frequency). The results are reported in Fig. 11, where the differences between the positive and negative electrodes are showed both with the device completely discharged (Fig. 11a) and at different states of charge (Fig. 11c and d). The first thing to notice is the clear difference between the imaginary part of

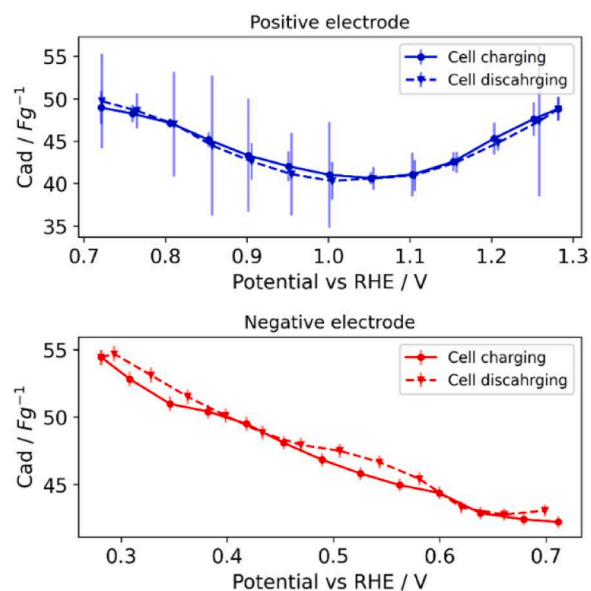


Fig. 10. Adsorption capacitance extracted from equivalent circuit model regression for both electrodes. Note that positive electrode potential spans from low to high during the device's charge while the one for the negative spans from high to low.

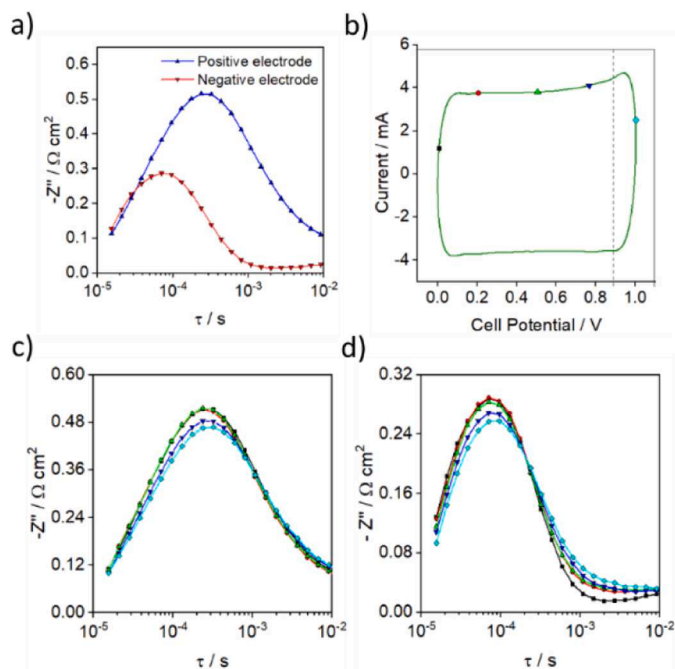


Fig. 11. Analysis of the imaginary part of the impedances for both electrodes. (a) comparison between $-Z''$ of positive and negative electrode, (b) current – potential profile of a voltammetry cycle with highlighted the points at which the profiles of the positive (c) and negative (d) electrodes are taken

the impedance of the two electrodes while completely discharged: both present a broad band at low time constants (high frequencies), but while the positive electrode is peaked at 274 μs with 1.77 s as full width half maximum (obtained by fitting the peak with a Gaussian function), the negative one is centered around 72 μs with 1.25 s as FWHM. This means that the adsorption process that occurs on the positive electrode is almost four times faster than the one on the negative side, but also that the time constant of such process is not unique but rather distributed over a broad spectrum. This time constants dispersion, as earlier

mentioned in Section 3.3, can be related to porosity. The evolution of the imaginary part of the impedance during cycling can also be analysed and discussed. For both electrodes, the peak related to the relaxation time of the adsorption process broadens and its maximum increases while charging. This can be better observed in Figs. 12 and 13, where the value of the peak time constant and FWHM evaluated by fitting the band with a Gaussian function are reported. It is once again possible to observe a clear dependence of an impedance-related variable, in this case τ , from the cell potential: its value, in fact, remains almost constant for both electrode throughout the whole cycling process apart from when the potential reaches values bigger than 0.7 V (positive electrode potentials around 1.2 V vs RHE), where τ grows significantly for the positive electrode, probably because of the presence of side-reactions (i.e. oxygen evolution).

4. Recommendations for experimental design

Dynamic Impedance Spectroscopy is a hyphenated combination of techniques usually performed separate, hence, to obtain a proper measurement a few cautions should be observed.

One of the main sources of spectral inconsistency when performing the DMFA is the interference between the DC component (e.g. scan rate for a cyclic voltammetry) of the signal and those produced by the lowest frequencies of the multisine. This can be clearly observed in the frequency-domain representation in Fig. 6: depending on the intensity, frequency and shape of the DC component of the signal (e.g. square, triangular), the skirt of its frequency representation can overlap more or less with the sub-Hz components of the multisine, thus adding a possible bias to the extracted impedance in the low frequency band. For this reason, it is important to tune the DC signal and the multisine so that they are separated enough in terms of frequencies. For quasi-triangular waves, a DC signal 25–50 times slower than the slowest component of the multisine is generally separated enough from the other so to avoid overlapping.

Another issue related to the use of Dynamic Electrochemical Impedance Spectroscopy is that of the low density of frequency points in the lower region. In fact, the frequency-dependant information is logarithmically spaced but to avoid intermodulation not all the harmonics have to be taken. This requirement reduces the number of frequencies that can be selected in the neighborhood of the base harmonic.

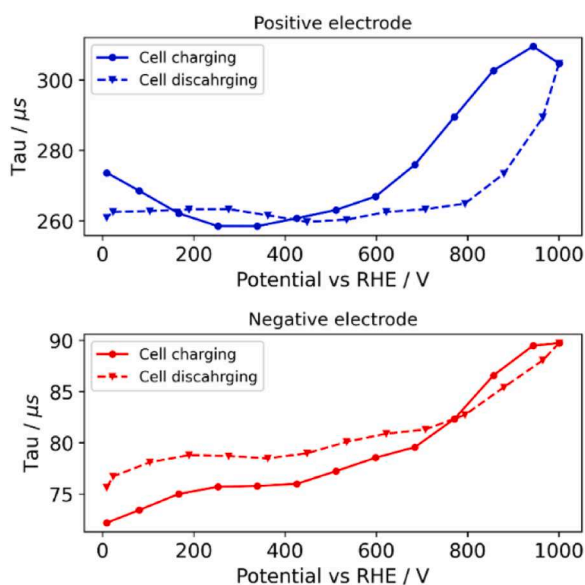


Fig. 12. Time constant (Tau) of the adsorption process extracted as the peak of Gaussian regression of the imaginary part of the time-varying impedance plotted against time for both electrodes.

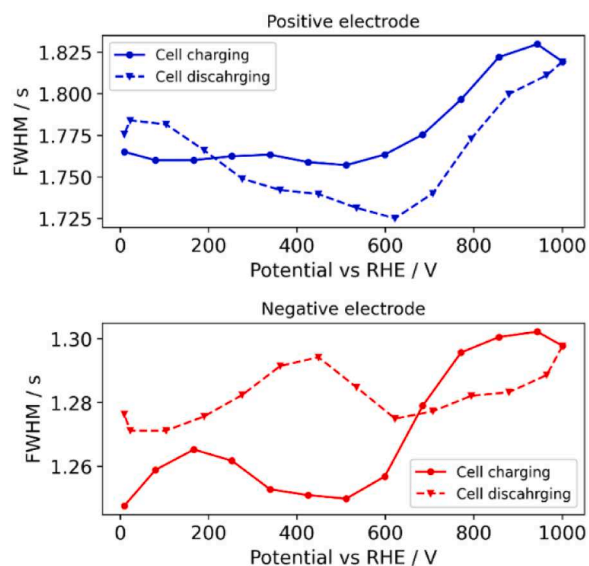


Fig. 13. Full width at half maximum of the Gaussian function regressed on the peak of the imaginary part of the time-varying impedance plotted against time for both electrodes.

Unfortunately, also the most interesting information lies in the low frequency band.

Lastly, the DMFA approach rely on the application of DFT algorithms on the whole signal. If the sampling frequency and/or the acquisition time are big (the number of points is the product of the two), the allocation of the signal in the memory of the computer can overflow the hardware capability. For example, in this work 2 cycles were acquired in one measurement (approximately 4 h long) collecting 500MSa with single precision (2 GB per signal) using a typical lab PC equipped with 16GB of RAM.

5. Conclusion

In this paper, the capability of the Dynamic Electrochemical Impedance Spectroscopy (DEIS) to collect kinetic information of a symmetric Electrochemical Double Layer Capacitor (EDLC) during cycling is presented. The impedance was computed from the multi-frequency potential and current signals using the Dynamic Multi-Frequency Analysis (DMFA), an easy-implementable algorithm. This approach allowed for the extraction of impedance spectra operando in a relatively fast system (e.g. 8 mV s^{-1} , 4 mHz) while collecting impedance at low frequency (down to 300mHz after data cleaning), enough to analyze the capacitive behavior of the cell. The novel use of two synchronized channels of a potentiostat together with the inclusion of a reference electrode allowed for the simultaneous measurement of the impedances of both the active electrodes of the EDLC, while charging and discharging the device imposing a potential sweep between them, thus emulating a real device. The extracted time-varying impedance was used to evaluate: (i) the kinetic parameters evolution from an equivalent circuit (EC) regression, (ii) time constants from graphical analysis; for both electrodes during the potential scan. The former gave a value of the average capacitance compatible with the one calculated with a simple formula based on the scan rate (see Eq. (1)). In addition, the presence of side reactions while approaching the water oxidation potential was observed by the impedance response. The values of the parameters extracted from the equivalent circuit are strongly different between the two active electrodes even though the material is chemically identical, showing a strong dependence on the working potential and on the precedent history of the electrode itself (e.g. pre-treatments). The latter highlights instead the difference in the time constant of the adsorption process of the two electrodes and its dependence, again, with the

working potential and precedent history. The present work is a proof of concept for the use of the DEIS in three-electrode configuration compact cells to characterize the kinetics of the electrodes. The proposed approach can be also extended to more complicated systems like batteries, which share the same cell design, and are undoubtedly a trending topic in science and industry that can benefit from the use of more operando information.

Funding

This work was supported by the Fraunhofer Internal Programs under Grant No. Attract 028-602604 ProLIBs and European Research Council (ERC) under European Union's Horizon 2020 research and innovation program Consolidator Grant No. 772579 EllonT.

CRediT authorship contribution statement

Nicolò Pianta: Investigation, Data curation, Methodology, Writing – original draft, Writing – review & editing, Software. **Federico Scarpioni:** Software, Formal analysis, Data curation, Visualization, Writing – review & editing. **Richard Chukwu:** Data curation, Software. **Fabio La Mantia:** Conceptualization, Methodology, Software, Resources, Supervision. **Riccardo Ruffo:** Conceptualization, Supervision, Project administration.

Declaration of Competing Interest

The authors declare that they have no known competing financial interests or personal relationships that could have appeared to influence the work reported in this paper.

Data availability

Data will be made available on request.

References

- M. Winter, R.J. Brodd, What are batteries, fuel cells, and supercapacitors? *Chem. Rev.* 104 (2004) 4245–4269, <https://doi.org/10.1021/cr020730k>.
- A. Burk, Ultracapacitors: why, how, and where is the technology, *J. Power Sources* 91 (2000) 37–50. <http://www.sciencedirect.com/science/article/pii/S0378775300004857> %5Cnpapers3://publication/livfe/id/55939.
- L.L. Zhang, X.S. Zhao, Carbon-based materials as supercapacitor electrodes, *Chem. Soc. Rev.* 38 (2009) 2520–2531, <https://doi.org/10.1039/b813846j>.
- J.R. Miller, P. Simon, *Electrochem. Capacit. Energy Manag. Sci.* 321 (2008) 651–653 (80-).
- A.A. Moya, Identification of characteristic time constants in the initial dynamic response of electric double layer capacitors from high-frequency electrochemical impedance, *J. Power Sources* 397 (2018) 124–133, <https://doi.org/10.1016/j.jpowsour.2018.07.015>.
- A.S. Bandarenka, Exploring the interfaces between metal electrodes and aqueous electrolytes with electrochemical impedance spectroscopy, *Analyst* 138 (2013) 5540–5554, <https://doi.org/10.1039/c3an00791j>.
- K. Mc Carthy, H. Gullapalli, K.M. Ryan, T. Kennedy, Review—use of impedance spectroscopy for the estimation of li-ion battery state of charge, state of health and internal temperature, *J. Electrochem. Soc.* 168 (2021), 080517, <https://doi.org/10.1149/1945-7111/ac1a85>.
- P. Iurilli, C. Brivio, V. Wood, On the use of electrochemical impedance spectroscopy to characterize and model the aging phenomena of lithium-ion batteries: a critical review, *J. Power Sources* 505 (2021), 229860, <https://doi.org/10.1016/j.jpowsour.2021.229860>.
- R.R. Gaddam, L. Katzenmeier, X. Lamprecht, A.S. Bandarenka, Review on physical impedance models in modern battery research, *Phys. Chem. Chem. Phys.* 23 (2021) 12926–12944, <https://doi.org/10.1039/d1cp00673h>.
- F. Luffrano, P. Staiti, M. Minutoli, Evaluation of nafion based double layer capacitors by electrochemical impedance spectroscopy, *J. Power Sources* 124 (2003) 314–320, [https://doi.org/10.1016/S0378-7753\(03\)00589-5](https://doi.org/10.1016/S0378-7753(03)00589-5).
- X. Liu, L. Juan, L. Zhan, L. Tang, Y. Wang, W. Qiao, X. Liang, L. Ling, Effect of conductive filler on the impedance behaviors of activated carbon based electric double layer capacitors, *J. Electroanal. Chem.* 642 (2010) 75–81, <https://doi.org/10.1016/j.jelechem.2010.02.008>.
- O. Bohlen, J. Kowal, D.U. Sauer, Ageing behaviour of electrochemical double layer capacitors. Part I. Experimental study and ageing model, *J. Power Sources* 172 (2007) 468–475, <https://doi.org/10.1016/j.jpowsour.2007.07.021>.
- M.R. Hasyim, D. Ma, R. Rajagopalan, C. Randall, Prediction of charge-discharge and impedance characteristics of electric double-layer capacitors using porous electrode theory, *J. Electrochem. Soc.* 164 (2017) A2899–A2913, <https://doi.org/10.1149/2.0051713jes>.
- P. Agarwal, M.E. Orazem, L.H. Garcia-Rubio, Application of measurement models to impedance spectroscopy: III. Evaluation of consistency with the Kramers-Kronig relations, *J. Electrochem. Soc.* 142 (1995) 4159–4168, <https://doi.org/10.1149/1.2048479>.
- T. Pajkossy, M.U. Ceblin, G. Mészáros, Dynamic electrochemical impedance spectroscopy for the charge transfer rate measurement of the ferro/ferricyanide redox couple on gold, *J. Electroanal. Chem.* 899 (2021) 1–8, <https://doi.org/10.1016/j.jelechem.2021.115655>.
- P. Slepiski, K. Darowicki, E. Janicka, A. Sierczynska, Application of electrochemical impedance spectroscopy to monitoring discharging process of nickel/metal hydride battery, *J. Power Sources* 241 (2013) 121–126, <https://doi.org/10.1016/j.jpowsour.2013.04.039>.
- K. Darowicki, P. Slepiski, M. Szociński, Novel application of dynamic electrochemical impedance monitoring to a cathoporetic coating process, *Prog. Org. Coat.* (2020) 149, <https://doi.org/10.1016/j.porgcoat.2020.105906>.
- K. Darowicki, J. Orlikowski, A. Arutunow, W. Jurczak, The effect of tensile stresses on aluminium passive layer durability, *Electrochim. Acta* 51 (2006) 6091–6096, <https://doi.org/10.1016/j.electacta.2005.12.054>.
- A. Battistel, F.L. Mantia, On the physical definition of dynamic impedance: how to design an optimal strategy for data extraction, *Electrochim. Acta* 304 (2019) 513–520, <https://doi.org/10.1016/j.electacta.2019.03.033>.
- N. Hallemaans, R. Pintelon, E. Van Gheem, T. Collet, R. Claessens, B. Wouters, K. Ramharter, A. Hubin, J. Lataire, Best linear time-varying approximation of a general class of nonlinear time-varying systems, *IEEE Trans. Instrum. Meas.* 70 (2021), <https://doi.org/10.1109/TIM.2021.3086891>.
- K.J. Szekeeres, S. Vesztergom, M. Ujvári, G.G. Láng, Methods for the determination of valid impedance spectra in non-stationary electrochemical systems: concepts and techniques of practical importance, *ChemElectroChem* 8 (2021) 1233–1250, <https://doi.org/10.1002/celec.202100093>.
- M. Tribbia, N. Pianta, G. Bruggen, R. Lorenzi, R. Ruffo, A new double layer supercapacitor made by free-standing activated carbon membranes and highly concentrated potassium acetate solutions, *Electrochim. Acta* 364 (2020), 137323, <https://doi.org/10.1016/j.electacta.2020.137323>.
- M. Pasta, A. Battistel, F.L. Mantia, Lead-lead fluoride reference electrode, *Electrochem. Commun.* 20 (2012) 145–148, <https://doi.org/10.1016/j.elecom.2012.04.018>.
- D. Koster, G. Du, A. Battistel, F.L. Mantia, Dynamic impedance spectroscopy using dynamic multi-frequency analysis: a theoretical and experimental investigation, *Electrochim. Acta* 246 (2017) 553–563, <https://doi.org/10.1016/j.electacta.2017.06.060>.
- R. Chukwu, J. Mugisa, D. Brogioli, F.L. Mantia, Statistical analysis of the measurement noise in dynamic impedance spectra, *ChemElectroChem* (2022), 202200109, <https://doi.org/10.1002/celec.202200109>.
- A. Battistel, M. Fan, J. Stojadinović, F.L. Mantia, Analysis and mitigation of the artefacts in electrochemical impedance spectroscopy due to three-electrode geometry, *Electrochim. Acta* 135 (2014) 133–138, <https://doi.org/10.1016/j.electacta.2014.05.011>.
- G. Hsieh, T.O. Mason, E.J. Garboczi, L.R. Pederson, Experimental limitations in impedance spectroscopy: part III. Effect of reference electrode geometry/position, *Solid State Ion.* 96 (1997) 153–172, [https://doi.org/10.1016/S0167-2738\(97\)00073-8](https://doi.org/10.1016/S0167-2738(97)00073-8).
- R. Raccichini, M. Amores, G. Hinds, Critical review of the use of reference electrodes in li-ion batteries: a diagnostic perspective, *Batteries* 5 (2019) 1–24, <https://doi.org/10.3390/batteries5010012>.
- I. Frateur, V.M.W. Huang, M.E. Orazem, N. Pébère, B. Tribollet, V. Vivier, Local electrochemical impedance spectroscopy: considerations about the cell geometry, *Electrochim. Acta* 53 (2008) 7386–7395, <https://doi.org/10.1016/j.electacta.2008.01.012>.
- A. Janes, H. Kurig, E. Lust, Characterization of activated nanoporous carbon as electrical double layer capacitor electrode materials, *ECS Trans.* 3 (2007) 39–48, <https://doi.org/10.1149/1.2795234>.
- A. Lasia, The origin of the constant phase element, *J. Phys. Chem. Lett.* 13 (2022) 580–589, <https://doi.org/10.1021/acs.jpcclett.1c03782>.
- S.J. Cooper, A. Bertei, D.P. Finegan, N.P. Brandon, Simulated impedance of diffusion in porous media, *Electrochim. Acta* 251 (2017) 681–689, <https://doi.org/10.1016/j.electacta.2017.07.152>.
- A. Eftekhari, Surface diffusion and adsorption in supercapacitors, *ACS Sustain. Chem. Eng.* 7 (2019) 3692–3701, <https://doi.org/10.1021/acssuschemeng.8b01075>.
- A. Murari, E. Peluso, F. Cianfrani, P. Gaudio, M. Lungaroni, On the use of entropy to improve model selection criteria, *Entropy* 21 (2019) 1–12, <https://doi.org/10.3390/e21040394>.
- B. Hirschorn, M.E. Orazem, B. Tribollet, V. Vivier, I. Frateur, M. Musiani, Determination of effective capacitance and film thickness from constant-phase-

- element parameters, *Electrochim. Acta* 55 (2010) 6218–6227, <https://doi.org/10.1016/j.electacta.2009.10.065>.
- [36] M.E. Orazem, N. Pébère, B. Tribollet, Enhanced graphical representation of electrochemical impedance data, *J. Electrochem. Soc.* 153 (2006) B129, <https://doi.org/10.1149/1.2168377>.
- [37] M. Heinzmann, A. Weber, E. Ivers-Tiffée, Advanced impedance study of polymer electrolyte membrane single cells by means of distribution of relaxation times, *J. Power Sources* 402 (2018) 24–33, <https://doi.org/10.1016/j.jpowsour.2018.09.004>.